

STAEBLE: A surface-temperature- and available-energy-based lake evaporation model

Nelson Luís Dias¹, Lucas Emilio Bernardelli Hoeltgebaum¹, and Irani dos Santos²

¹Federal University of Paraná

²Federal University of Parana, Brazil

November 24, 2022

Abstract

A mass transfer evaporation model is proposed that uses MODIS water surface temperature data and land-based meteorological data, and employs a new approach to calibrate the transfer coefficient via closure of the long-term energy budget of the lake. Some of the longstanding issues of developing and applying lake evaporation models are reviewed, including the adequacy of using land-based meteorological data, the difficulty of applying transfer coefficients with fixed values calibrated elsewhere, and the need to estimate rates of change of stored enthalpy when the model involves energy budget concepts. Publicly available data from a 5-year measurement campaign at Lake Mead allow to quantify the effect of using land-based data, and subsequently to test the proposed model. We show that atmospheric stability effects are very important, and that their incorporation by means of existing stability functions in the literature produces good results with a one-parameter model that can be locally calibrated with the same input data used by the model, without the need of local evaporation measurements. The model is simple in its structure and data requirements, and can be widely applied.

1 **STAEBLE: A surface-temperature- and**
2 **available-energy-based lake evaporation model**

3 **Nelson Luís Dias¹, Lucas E. B. Hoeltgebaum², Irani Santos³**

4 ¹Federal University of Paraná (UFPR), Environmental Engineering Departament*

5 ²Federal University of Paraná (UFPR), Graduate Program of Environmental Engineering

6 ³Federal University of Paraná (UFPR), Geography Department

7 **Key Points:**

- 8 • A new mass transfer method for lake evaporation is proposed that self-calibrates
9 the transfer coefficient
- 10 • The calibration is based on closing the long-term energy budget and dispenses in-
11 situ evaporation measurements
- 12 • Standard atmospheric stability functions must be incorporated for the best results

*Current address: Rua Francisco H. dos Santos, nº 210 Centro Politécnico / Setor de Tecnologia / Departamento de Engenharia Ambiental Jardim das Américas – Curitiba PR Brazil CEP 81531-980, Caixa Postal 19011 Edifício de Administração 3º andar

Corresponding author: Nelson L. Dias, nelsonluisdias@gmail.com

Abstract

A mass transfer evaporation model is proposed that uses MODIS water surface temperature data and land-based meteorological data, and employs a new approach to calibrate the transfer coefficient via closure of the long-term energy budget of the lake. Some of the longstanding issues of developing and applying lake evaporation models are reviewed, including the adequacy of using land-based meteorological data, the difficulty of applying transfer coefficients with fixed values calibrated elsewhere, and the need to estimate rates of change of stored enthalpy when the model involves energy budget concepts. Publicly available data from a 5-year measurement campaign at Lake Mead allow to quantify the effect of using land-based data, and subsequently to test the proposed model. We show that atmospheric stability effects are very important, and that their incorporation by means of existing stability functions in the literature produces good results with a one-parameter model that can be locally calibrated with the same input data used by the model, without the need of local evaporation measurements. The model is simple in its structure and data requirements, and can be widely applied.

Plain Language Summary

The evaporation rate from a natural or artificial lake (the amount of water that is evaporated into the atmosphere in a given time, from 1 day to 1 year) is an important quantity to model and understand the weather and climate, to model the water temperature in the lake, and for water resources management in general. It is also difficult to measure, and very uncertain to estimate. We developed a model that uses simple physics based on surface water temperature measured by satellite and local meteorological measurements, and that adjusts the total evaporation over many years to be equivalent to the total energy available to convert liquid water to vapor.

1 Introduction

Natural and artificial lakes are a common part of the landscape, and essential for human life, in their multiple uses for recreation, water supply for industry, irrigation and domestic use, energy generation, etc.; they also act as “sentinels” and integrators of terrestrial and atmospheric processes (Williamson et al., 2008), and play an important role in the emission of greenhouse gases to the atmosphere (DelSontro et al., 2018). The latent and sensible heat fluxes (and attendant water vapor mass flux) between the water

44 surface of lakes and the atmosphere are needed as boundary conditions for atmospheric
45 models and to quantify water losses. They are also used as boundary conditions in mod-
46 els for the evolution of the water temperature (see Hostetler & Bartlein, 1990), which
47 plays a fundamental control on all biochemical processes occurring in the lake’s body.

48 For well-known hydrological and environmental reasons, therefore, reliable lake evap-
49 oration estimates remain at the centerstage of water resources management, and even
50 more so in the face of increased water demand and scarcity, and climate change (Veldkamp
51 et al., 2017; Wang et al., 2018). Consequently, the need persists for reliable operational
52 estimates of lake evaporation, *i.e.*, estimates than can use readily available environmen-
53 tal data and can be applied as widely as possible, at timescales ranging from daily to yearly.

54 It is in the nature of the underlying physical processes, however, that the best flux
55 measurements or model-based estimates are derived from data collected directly above
56 the water surface: the physical basis for this fact is modernly provided by Monin-Obukhov
57 Similarity Theory (MOST) (Obukhov, 1946 1971). This is true of both the Energy-Budget
58 Bowen Ratio Method (Bowen, 1926; Brutsaert, 1982, Chapter 10) and the Eddy Covari-
59 ance Method (Swinbank, 1951; Brutsaert, 1982, Chapter 8), as well as many heat and
60 mass transfer methods and Penman (1948)’s combination method. This experimental
61 complicating factor is compounded, in the case of lakes, by the need to measure or es-
62 timate the rate of change of enthalpy stored in the lake’s waters by means of water tem-
63 perature profiles. Due to the limits in the accuracy of temperature measurements and
64 in spatial coverage, the deeper the lake, the longer is the time interval needed to derive
65 accurate enough estimates of change of enthalpy (Dias & Reis, 1998; Reis & Dias, 1998).

66 Of course, it is not impossible to perform in-lake measurements, as the early stud-
67 ies at lakes Hefner and Mead showed (USGS, 1954, 1958); several such studies at impor-
68 tant lakes around the world have been conducted since then (*e.g.* Omar & El-Bakry, 1981;
69 Assouline & Mahrer, 1993; Blanken et al., 2000; Cancelli et al., 2012; M. T. Moreo & Swan-
70 car, 2013; Armani et al., 2020). In this work, we concentrate on the particularly long 5-
71 year data set generated by the recent USGS Lake Mead study initially reported by M. T. Moreo
72 and Swancar (2013).

73 Because over-water measurements over extended periods are rare, in practice op-
74 erational lake evaporation models have had to rely, at least partly, on data measured at
75 meteorological stations over land. An early example is the hybrid method proposed by

76 Harbeck (1962), which combines water surface temperature and wind measured over the
77 water with vapor pressure measured upwind on land. Harbeck proposed a mass trans-
78 fer coefficient dependent on the lake’s surface area. This approach was corroborated the-
79 oretically in some measure by Brutsaert and Yeh (1970). Much later, McJannet et al.
80 (2012) compiled data for several water bodies and proposed a similar mass transfer co-
81 efficient, but with the wind measured over land. In practice, however, it appears that
82 the mass transfer coefficient is still too dependent on local conditions for a pure mass
83 transfer approach to be successful using a “universal” coefficient (*i.e.* a coefficient with
84 fixed values independent of location, even with an area dependence). Most models that
85 achieved some degree of success, therefore, relied to some extent on the energy-budget
86 or related approaches. For instance, Kohler and Parmele (1967) adapted Penman’s com-
87 bination approach; Morton (1983, 1986) used the combination approach to derive a sur-
88rogate of surface water temperature (then literally impossible to obtain in practice) and
89 use it in a slightly modified form of the Priestley-Taylor equation (Priestley & Taylor,
90 1972); more recently, water surface temperature has become available from remote sens-
91 ing, and Zhao et al. (2020) proposed a model that uses MODIS water surface temper-
92 ature data and Penman’s equation, together with McJannet et al.’s mass transfer coef-
93 ficient as well as Hostetler and Bartlein (1990)’s model for the evolution of water tem-
94 perature profiles, to estimate the rate of change of stored enthalpy.

95 In all cases cited above (except for Harbeck’s purely mass transfer approach), there
96 is a need to estimate the rate of change of enthalpy by various means because contin-
97 uous and sufficiently dense (in time and space) profiles of water temperature are gen-
98 erally not available. Moreover, although site-specific studies of turbulence over water con-
99 firm a strong dependence of mass and heat transfer coefficients on atmospheric stabil-
100 ity (as predicted by MOST) at the scale of 30 minutes – 1 hour (*e.g.* Verburg & Antenucci,
101 2010; Dias & Vissotto, 2017), all operational evaporation models described above use fixed
102 values and do not take into account atmospheric stability in the mass transfer coefficient.

103 In this work, we propose a different combination of physical principles. First, we
104 use on-land meteorological data together with MODIS water surface temperature in the
105 mass and heat transfer equations. Although there is some physical basis for this approach,
106 provided by the Brutsaert and Yeh (1970) study, we employ it empirically (as all oper-
107 ational lake evaporation models are forced to do) but verify it using the recent USGS
108 experimental campaign at lake Mead (M. T. Moreo & Swancar, 2013), showing that it

109 is quite reasonable in practice, even under rather extreme changes from the arid surround-
 110 ings to over-water conditions. Then we investigate the extent to which net radiation es-
 111 timates based on over-land data and MODIS water surface temperatures can replicate
 112 over-water measurements, and show that it is enough to use a suitably parameterized
 113 downwelling atmospheric radiation model. We propose to constrain the mass and heat
 114 transfer coefficients by imposing that the *long-term* energy budget of the lake be closed,
 115 effectively avoiding the need to calculate rates of change of enthalpy. This provides a lo-
 116 cal calibration of the mass and heat transfer coefficient, circumventing the use of a “uni-
 117 versal” transfer coefficient with fixed parameters. Finally, we assess the performance of
 118 five versions of the approach, and show that a model that takes into account atmospheric
 119 stability via the Businger-Dyer integral Monin-Obukhov functions for momentum and
 120 scalars, and a constant “effective” surface roughness obtained from the long-term energy-
 121 budget constraint is the best choice.

122 2 Theory and proposed model

123 In this work, all symbols used should be considered daily averages unless otherwise
 124 noted. Most of the equations, however, are strictly valid at the much shorter scale of 30
 125 minutes to 1 hour, according to MOST. The use of daily values is a compromise in the
 126 interest of simplicity and the ability to use more widely available data, but, as we shall
 127 see, atmospheric stability is still crucial at the daily time scale. In particular, care should
 128 be exercised when trying to interpret physically the turbulent scales u_* , θ_* and q_* de-
 129 fined below: it is better to consider them auxiliary values that, because they are derived
 130 from mixed over-land meteorological data and over-water surface temperatures at the
 131 daily timescale, do not necessarily carry their original meaning in MOST. All equations
 132 are written in the S.I. system of units; temperatures, therefore, should be entered in Kelvins.
 133 In the figures and in some temperature ranges, however, we use the auxiliary S.I. unit
 134 degree Celsius ($^{\circ}\text{C}$).

135 The energy-budget equation at the water surface of the lake is

$$136 \quad R_n = H + LE + D, \quad (1)$$

137 where R_n is the net radiation, H is the sensible heat flux, LE is the latent heat flux which
 138 is the product of $L = 2.464 \times 10^6 \text{ J kg}^{-1}$, the latent heat of evaporation, and E , the
 139 water vapor mass flux, and D is the rate of change of enthalpy stored in the lake’s wa-

140 ter. For simplicity, in the model L is kept constant at its nominal value at 15°C . Note
 141 that (1) implicitly neglects the ground heat flux at the lake's bottom. Net radiation is
 142 estimated from

$$143 \quad R_n = R_s(1 - \alpha) + \epsilon R_a - \epsilon \sigma T_0^4, \quad (2)$$

144 where R_s is (the directly retrieved or measured) downwelling solar radiation, α is the
 145 water's albedo, $\epsilon = 0.97$ is the water's absorptivity/emissivity, R_a is downwelling long-
 146 wave radiation, $\sigma = 5.67037 \times 10^{-8} \text{ W m}^{-2} \text{ K}^{-4}$ is Stefan-Boltzmann's constant, and
 147 T_0 is the water surface temperature. The daily albedo is interpolated for each day and
 148 the local latitude from Table 5 of Cogley (1979), whose values are nominally placed at
 149 the 15th day of each month.

150 The clear-sky downwelling atmospheric radiation is estimated with Brutsaert (1975a)'s
 151 equation, *viz.*

$$152 \quad R_{ac} = \epsilon_{ac} \sigma T_a^4, \quad \epsilon_{ac} = a_B \left(\frac{e_a}{T_a} \right)^{b_B}, \quad (3)$$

153 where a_B and b_B are constants that vary somewhat with location. The actual downwelling
 154 atmospheric radiation is then obtained with the help of Bolz's equation (Brutsaert, 1982,
 155 Section 6.1),

$$156 \quad R_a = (1 + 0.22C^2) R_{ac} \quad (4)$$

157 where the cloudiness C is obtained indirectly by solving for S in Prescott's (Brutsaert,
 158 1982, Section 6.1) equation:

$$159 \quad C = 1 - S, \quad R_s = R_{se}(a_P + b_P S), \quad (5)$$

160 where a_P and b_P vary with location, S is sunshine duration, and R_{se} is mean daily so-
 161 lar radiation at the top of the atmosphere (Sellers, 1965, Chapter 3),

$$162 \quad R_{se} = \left(\frac{r_a}{r} \right)^2 \frac{R_{s0}}{\pi} [H \sin \delta \sin \phi + \cos \delta \cos \phi \sin H], \quad (6)$$

163 where $R_{s0} = 1361.5 \text{ W m}^{-2}$ is the solar constant, r_a is the semi-major axis of the Earth's
 164 orbit (1 astronomical unit), r is the Sun-Earth distance on a given day, ϕ is the latitude,
 165 δ is the declination of the Sun on a given day, and

$$166 \quad H = \arccos(-\tan(\phi) \tan(\delta)) \quad (7)$$

167 is half the duration of the day in radians. For each day, r/r_a and δ are calculated from
 168 van Flandern and Pulkkinen (1979).

169 Here, we chose (3) on the basis of its good performance among several studies, in-
 170 cluding Sugita and Brutsaert (1993), Prata (1996), Duarte et al. (2006) and Choi et al.
 171 (2008). Note that in Sugita and Brutsaert (1993), Duarte et al. (2006) and Choi et al.
 172 (2008) the constants a_B and b_B were locally calibrated. It should also be noted that nowa-
 173 days values of R_a can be retrieved from reanalysis data. Here, however, we prefer to es-
 174 timate it as it would have to be if meteorological data were obtained from an actual me-
 175 teorological station close to the lake.

176 In the proposed model, H and LE are calculated at the daily time scale from stan-
 177 dard heat and mass transfer equations:

$$178 \quad H = \rho c_p f(u, \theta)(T_0 - T_a), \quad (8)$$

$$179 \quad LE = \rho c_p f(u, \theta) \frac{(e_0 - e_a)}{\gamma} = \rho L f(u, \theta)(q_0 - q_a), \quad (9)$$

180 where ρ is the dry air density at the nominal pressure P and temperature T of the lo-
 181 cation's altitude h in a standard atmosphere (COESA, 1976):

$$183 \quad T = T_s - 0.0065h, \quad (10)$$

$$184 \quad P = P_s \left[\frac{T}{T_s} \right]^{5.256}, \quad (11)$$

$$185 \quad \rho = \frac{P}{R_d T}, \quad (12)$$

186 with $P_s = 101325$ Pa and $T_s = 288.15$ K; $c_p = 1005$ J kg⁻¹K⁻¹ is the specific heat
 187 of dry air, $R_d = 287.038$ J kg⁻¹K⁻¹ is the dry air constant, and $\gamma = c_p P / (0.622L)$ is
 188 the psychrometric constant. We use a nominally constant ρ calculated for dry air on the
 189 grounds of simplicity, as this has little impact on the results. In (8)–(9), u is the wind
 190 speed at 10 m over land; T_a is the air temperature at 2 m over land; e_0 and q_0 are the
 191 saturation vapor pressure and specific humidity at the water surface temperature T_0 ; and
 192 e_a and q_a are the water vapor pressure and specific humidity at 2 m over land.
 193

194 So far, equations (2)–(12) completely specify the model (assuming suitable values
 195 of a_B , b_B , a_P and b_P are provided), except for the transfer coefficient or “wind function”
 196 $f(u, \theta)$, which is assumed to be the same for H and LE ; here θ is a parameter to be de-
 197 termined as follows. Consider a period of N days spanning an *exact* integer number of
 198 years. For example, in the dataset of this study the period goes from March 1st 2010 to
 199 February 28th 2015 and $N = 1826$ days. Then, we sum (1) over this period and impose

$$200 \quad \sum_{i=1}^N D_i = 0 \Rightarrow \sum_{i=1}^N R_{ni} = \sum_{i=1}^N [H_i + LE_i]. \quad (13)$$

201 Using (8)–(9),

$$202 \quad \sum_{i=1}^N R_{ni} = \sum_{i=1}^N \rho c_p f(u_i, \theta) \left[(T_{0i} - T_{ai}) + \frac{e_{0i} - e_{ai}}{\gamma} \right]. \quad (14)$$

203 The constraint (13) is reasonable, provided that total volume changes are not too dras-
 204 tic between the beginning and the end of the period, and that advection effects can be
 205 neglected. Otherwise, it is in principle possible to make *ad-hoc* adjustments. Then, by
 206 solving (14) for θ , we effectively calibrate a local transfer coefficient: this is one of the
 207 main results in this work. Because there is only one degree of freedom, however, only
 208 a single-parameter $f(u, \theta)$ can be prescribed. The obvious advantage is that this produces
 209 a locally-calibrated transfer coefficient that takes into account local effects in an opti-
 210 mal way. Another advantage is that it completely eliminates the need to estimate the
 211 problematic term D since, once θ is obtained, the transfer equations (8)–(9) can be used
 212 directly. We call the resulting model “Surface-Temperature- and Available-Energy-Based
 213 Lake Evaporation” (STAEBLE), because it uses an extremely important physical con-
 214 trolling variable (the surface water temperature) and ensures long-term energy conser-
 215 vation.

216 We consider 5 alternatives for $f(u, \theta)$.

217 STAEBLE-A:

$$218 \quad f(u, \theta) = A, \quad (15)$$

219 where $\theta = A$ is obtained by direct substitution of (15) into (14):

$$220 \quad A = \frac{\sum_{i=1}^N R_{ni}}{\sum_{i=1}^N \rho c_p \left[(T_{0i} - T_{ai}) + \frac{(e_{0i} - e_{ai})}{\gamma} \right]}. \quad (16)$$

221 STAEBLE-B:

$$222 \quad f(u, \theta) = Bu, \quad (17)$$

223 where $\theta = B$ is obtained by direct substitution of (17) into (14):

$$224 \quad B = \frac{\sum_{i=1}^N R_{ni}}{\sum_{i=1}^N \rho c_p u_i \left[(T_{0i} - T_{ai}) + \frac{(e_{0i} - e_{ai})}{\gamma} \right]}. \quad (18)$$

225 STAEBLE-AB:

$$226 \quad f(u) = (A + Bu)/2, \quad (19)$$

227 where A and B are the previously obtained values in (16) and (18). STAEBLE-AB is
 228 an engineering compromise: because so many “Dalton-like” equations are of the form
 229 (19), we simply use the average of the previous two alternatives.

230 The next two alternatives are stability-dependent, and use standard MOST sta-
 231 bility functions. For each day, one solves iteratively the following set of equations for u_* ,
 232 T_* , q_* , and $\zeta_{a,b}$ (Brutsaert, 1982, Chapters 4 and 5):

$$233 \quad u_* = \frac{\kappa u}{\ln\left(\frac{z_b}{z_0}\right) - \Psi_u(\zeta_b)}, \quad (20)$$

$$234 \quad z_0 = a_C u_*^2 / g, \quad (21)$$

$$235 \quad z_{0+} = \frac{u_* z_0}{\nu}, \quad (22)$$

$$236 \quad z_{0s} = z_0 \exp\left(-2.25 z_{0+}^{1/4}\right), \quad (23)$$

$$237 \quad T_* = \frac{\kappa(T_0 - T_a)}{\ln\left(\frac{z_a}{z_{0s}}\right) - \Psi_s(\zeta_a)}, \quad (24)$$

$$238 \quad q_* = \frac{\kappa(q_0 - q_a)}{\ln\left(\frac{z_a}{z_{0s}}\right) - \Psi_s(\zeta_a)}, \quad (25)$$

$$239 \quad T_{v*} = (1 + 0.61q_a)T_* + 0.61T_a q_*, \quad (26)$$

$$240 \quad \zeta_{a,b} = -\frac{\kappa g z_{a,b} T_{v*}}{T_{va} u_*^2}, \quad (27)$$

242 where the virtual temperature is $T_{va} = T_a(1 + 0.61q_a)$. Given a value of a_C or z_0 (fixed
 243 during the iteration), (20)–(27) (with the possible omission of (21)) are repeatedly cal-
 244 culated until two consecutive values of $f(u, \theta)$ in (28) below differ by less than 10^{-6} (for
 245 STAEBLE-C) or 10^{-5} (for STAEBLE-CH); see definitions below. When convergence is
 246 achieved, the transfer coefficient is

$$247 \quad f(u, \theta) = \frac{\kappa^2 u}{\left[\ln\left(\frac{z_b}{z_0}\right) - \Psi_u(\zeta_b)\right] \left[\ln\left(\frac{z_a}{z_{0s}}\right) - \Psi_s(\zeta_a)\right]} \quad (28)$$

248 with the final values of z_0 , z_{0s} , ζ_a and ζ_b .

249 Above, Ψ_u and Ψ_s are the Businger-Dyer integral functions for wind and a scalar
 250 (Brutsaert, 1982, section 4.2). For completeness, the equations are given in Appendix
 251 A. The reference heights are $z_a = 2$ m for the scalars and $z_b = 10$ m for the wind, $\kappa =$
 252 0.4 is von Kármán’s constant, $g = 9.81 \text{ m s}^{-2}$ is the acceleration of gravity, and ζ_a and
 253 ζ_b are Obukhov’s stability variable calculated at z_a and z_b respectively. The scalar rough-
 254 ness is calculated in (22)–(23) according to Brutsaert (1975b) assuming rough turbulent
 255 flow, where ν is the kinematic viscosity of air calculated with T from (10) according to
 256 Montgomery (1947). Strictly speaking, (23) parameterizes the water vapor roughness length,
 257 but again for the sake of simplicity we use a single value for both LE and H .

258 At this point, $f(u, \theta)$ is reduced to a single-parameter model, which is either an “ef-
 259 fective” momentum roughness z_0 (we call it an effective roughness because it uses mixed

260 land-water variables in the transfer equations, blurring its physical meaning) or the (equally
 261 “effective”) Charnock parameter a_C . We tested two alternatives:

262 STAEBLE-C: where $\theta = z_0$ is assumed constant, in which case (21) is omitted.

263 STAEBLE-CH: where $\theta = a_C$ and z_0 is calculated for each day by (21).

264 In both cases, the parameter θ must be obtained by trial-and-error. We use a sim-
 265 ple bisection method (with logarithmically spaced midpoints) where either z_0 itself (in
 266 the case of STABLE-C) or a_C (in the case of STABLE-CH) is found iteratively by solv-
 267 ing (14) for the respective θ , until $\sum_{i=1}^N [H_i + LE_i] / \sum_{i=1}^N R_{ni} < 0.01$. In STAEBLE-
 268 C, the initial interval for the search of z_0 by the bisection method is $[2 \times 10^{-8} \text{ m}, 2 \text{ m}]$.
 269 In STAEBLE-CH, the initial interval for the search of a_C by the bisection method is
 270 $[2 \times 10^{-7}, 20]$.

271 The resulting model is parsimonious with data requirements (MODIS water surface
 272 temperature and on-land meteorological data, both at the daily time scale), calibrates
 273 the transfer coefficient $f(u, \theta)$ locally by enforcing that the long-term lake energy bud-
 274 get is closed without the need of local measurements of lake evaporation, and circum-
 275 vents the use of the rate-of-change of enthalpy D . The simplicity of the model should
 276 make it easy to apply at any location where the required data are available. We proceed
 277 to test it at Lake Mead.

278 **3 Test site and data**

279 To test the proposed model, we use the publicly available data (M. Moreo, 2015)
 280 from the recent Lake Mead USGS evaporation study first reported by M. T. Moreo and
 281 Swancar (2013). Lake Mead is located in Nevada and Arizona (36.25°N , 114.39°W) and
 282 is mainly fed by the Colorado River; it has a maximum surface area of 659.3 km^2 , a max-
 283 imum elevation of 374.6 m , and a total storage of 34.069 Mm^3 , being the largest Amer-
 284 ican reservoir by volume, and second by area. The climate is hot and arid. For more de-
 285 tails, see M. T. Moreo and Swancar (2013). The measured data from the study comprise
 286 5 years of continuously reported values of daily H , LE and R_n as well as air tempera-
 287 ture and relative humidity over the lake; and 32 months of water surface temperature
 288 at a floating platform close to Sentinel Island, from March 1st 2010 to October 30th 2012.
 289 The period of continuous flux measurements used here is from March 1st 2010 to Febru-
 290 ary 28th 2015. The reported fluxes were corrected to agree more closely to independen-

291 measured terms of the energy-budget of the lake (M. T. Moreo & Swancar, 2013, p. 28
292 and Table 8). Relatively important values of heat advection at Lake Mead for the pe-
293 riod March 2011 – February 2012 are reported, with an overall ratio of advected heat
294 to net radiation for the first two years of measurement of $14 \text{ W m}^{-2}/144 \text{ W m}^{-2} \approx 10\%$
295 (M. T. Moreo & Swancar, 2013, Table 4). Heat advection data are not published for the
296 whole period of measurements (5 years), however, and, as we will see, in the long run
297 the adjusted published fluxes very closely match measured net radiation. For this rea-
298 son, further consideration of heat advection is not made in this work.

299 For the same period and for each day, MODIS water surface temperature at 1 km
300 resolution is available from the AQUA and TERRA satellites. For each satellite, the daily
301 water surface temperature is taken as the mean of a daytime and a nighttime measure-
302 ment. If either one or the other of the two is missing, the daily mean is filled via linear
303 regression between the remaining value and the daily mean calculated with complete data.
304 When both daytime and nighttime values are missing, gaps are interpolated in time. Fi-
305 nally, the daily water surface temperature is taken as the mean of the two satellites’s tem-
306 perature data. We discarded points too close to land in the MODIS grid, and averaged
307 those closer to the center of the lake, as shown in yellow in Figure 1, to obtain a spa-
308 tially representative water surface temperature. We also used a single grid point from
309 the ERA5 reanalysis data at 31 km resolution (Hersbach et al., 2018, shown in black in
310 Figure 1) to obtain daily time series of air temperature, water vapor pressure (both at
311 a nominal height of 2 m), wind speed at 10 m, and solar radiation. Yang and Bright (2020)
312 report very good values of normalized mean bias error and normalized root mean square
313 error, of 0.93% and 14.17% respectively, for the ERA5 solar radiation product against
314 measured values of the Baseline Surface Radiation Network station of Desert Rock, Nevada,
315 which is approximately 131 km WNW of the Southern tip of Lake Mead.

316 The dataset provides a unique opportunity to verify the adequacy of several ap-
317 proximations inevitable in operational lake evaporation models partly based on over-land
318 measured or retrieved data. In our case, we will be able to investigate: (i) the quality
319 of the MODIS-derived water surface temperature compared to *in-situ* measurements; (ii)
320 the agreement between the accumulated measured energy fluxes and net radiation, and
321 the extent to which (13) is valid; (iii) the differences between over-land and over-water
322 T_a and e_a ; (iv) the impact of those differences on measured and estimated Bowen ratios;
323 (v) the adequacy of net radiation derived from (3)–(5) and ultimately (vi) the ability of

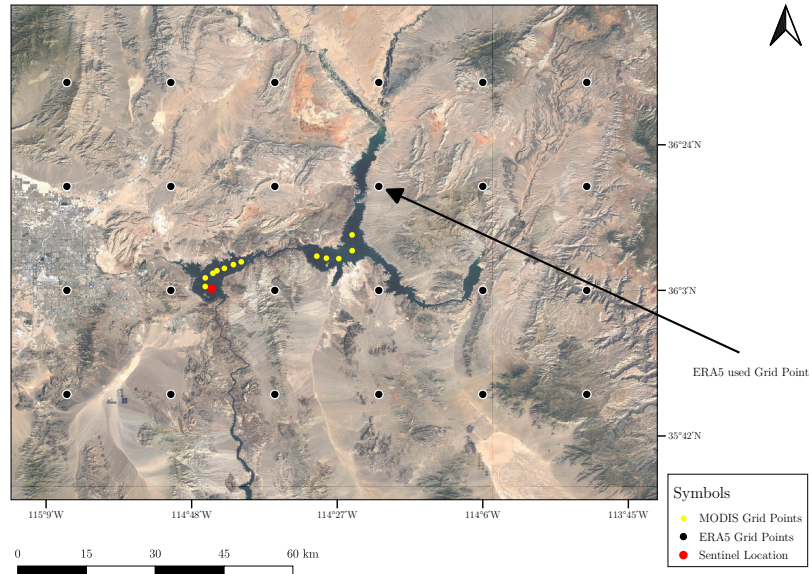


Figure 1. The retrieval of data from MODIS and ERA5 grids: black points indicate the ERA5 grid, and the arrow shows the particular grid point from which meteorological data were obtained; the yellow points are the MODIS grid points used to obtain a spatially-averaged T_0 . The red point shows the location of the Sentinel Island floating platform .

324 the transfer equations (8)–(9) using over-land data and MODIS-derived T_0 to provide
 325 adequate estimates of E at the daily, 12-day and monthly time scales.

326 4 Overview of Lake Mead data

327 Figure 2 shows a comparison between the measured surface temperatures at the
 328 Sentinel Island platform and the MODIS estimates. We consider the MODIS temper-
 329 ature at the pixel closest to Sentinel Island in Figure 2-a as well as the spatially-averaged
 330 value in Figure 2-b. The two resulting T_0 values from MODIS are remarkably similar,
 331 which shows that the spatial variability of T_0 is small. Using the T_0 spatial average in
 332 STAEBLE, therefore, is unlikely to bias the results, and from this point on “MODIS T_0 ”
 333 means the spatially-averaged values. The overall agreement between MODIS and mea-
 334 sured T_0 is generally good, except for the winter when MODIS tends to underestimate
 335 T_0 .

336 Figure 3 shows the cumulative values of the measured $H + LE$ and R_n : the dif-
 337 ference between the two is only 3%; this indicates an excellent agreement, which in no

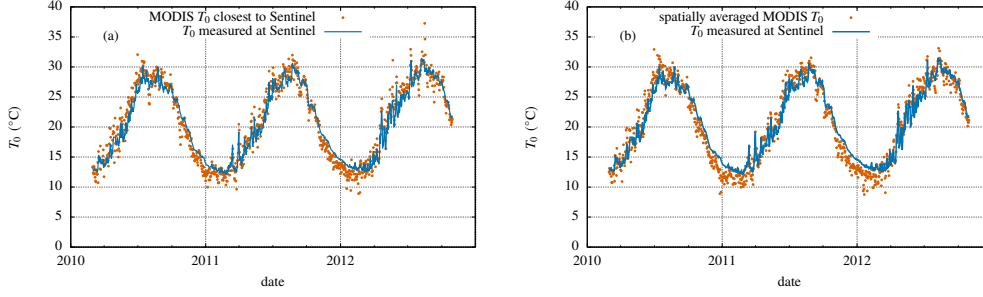


Figure 2. Comparison between measured water surface temperature and the Sentinel Island platform (blue line) versus (a) MODIS water surface temperature at the pixel closest to Sentinel and (b) spatially averaged MODIS water surface temperatures along the lake’s “center”.

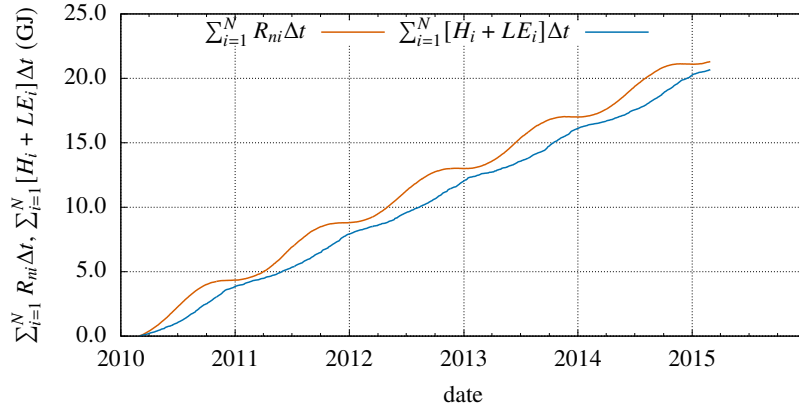


Figure 3. Cumulative values of measured H , LE and R_n .

338 doubt is partly due to the fact that H and LE were corrected to agree with the energy
 339 budget of the lake, as mentioned above.

340 A comparison between land and lake water vapor pressure and air temperature is
 341 given in figure 4. There is a substantial “lake effect” on vapor pressures, but much less
 342 on air temperatures. In hindsight, this is due to the smallness of the sensible heat flux
 343 over the lake. While the much larger water vapor flux affects the overlying air water va-
 344 por pressure significantly, it seems that the weak sensible heat flux is unable to produce
 345 an appreciable effect on air temperature. To the best of our knowledge, this may well
 346 be one of the longest data records available for such a comparison. This is obviously im-
 347 portant, as it allows to quantify how much we err in lake evaporation models due to lack
 348 of over-water data, as we will now assess in terms of Bowen ratios.

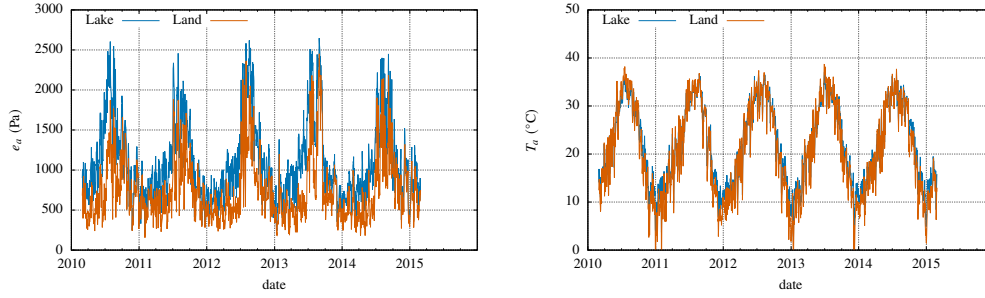


Figure 4. Comparison between lake and land values of water vapor pressure (left) and air temperature (right).

349 In the literature, it is sometimes expedient to differentiate between “flux” and “gra-
 350 dient” Bowen ratios, defined respectively by (Lang et al., 1983)

$$351 \quad \text{Bo}_f = \frac{H}{LE}, \quad \text{Bo}_g = \gamma \frac{T_0 - T_a}{e_0 - e_a}. \quad (29)$$

352 Clearly, the closer that Bo_g is to Bo_f , the better will the model partition energy between
 353 H and LE , and the better we expect our overall LE estimates to be.

354 Therefore, we compare Bowen ratios under two scenarios: (i) with T_0 given by the
 355 Sentinel platform measurements and (ii) with MODIS-derived T_0 . Both are calculated
 356 for the common 32-month period for which Sentinel data are available, and in each case
 357 we analyze two alternatives: Bo_g from lake data *versus* Bo_f and Bo_g from land data *ver-*
 358 *sus* Bo_f . The results are shown in Figure 5. The comparison of lake \times land data for the
 359 calculation of Bo_g (*i.e.* (a) \times (b) and (c) \times (d)) is fairly reassuring: although there are
 360 obvious differences (expected in view of the results shown in Figure 4), they are not too
 361 drastic. In other words, although it introduces biases, using land data to estimate Bowen
 362 ratios still produces reasonable results. The reliability of using MODIS T_0 instead of mea-
 363 sured T_0 at the Sentinel platform is slightly worse (*i.e.* comparing (a) with (c) and (b)
 364 with (d)), but still acceptable. The upshot is that, in spite of the caveat that according
 365 to MOST the transfer equations should be applied with in-lake measured data, the use
 366 of land-measured e_a and T_a and T_0 from MODIS at Lake Mead is still reasonable to es-
 367 timate Bowen ratios and may be enough for operational purposes. This is a conclusion
 368 that applies locally only, but the fact that Lake Mead is situated in an arid region, where
 369 land-lake contrasts are expected to be larger, also lends support to the idea that the use

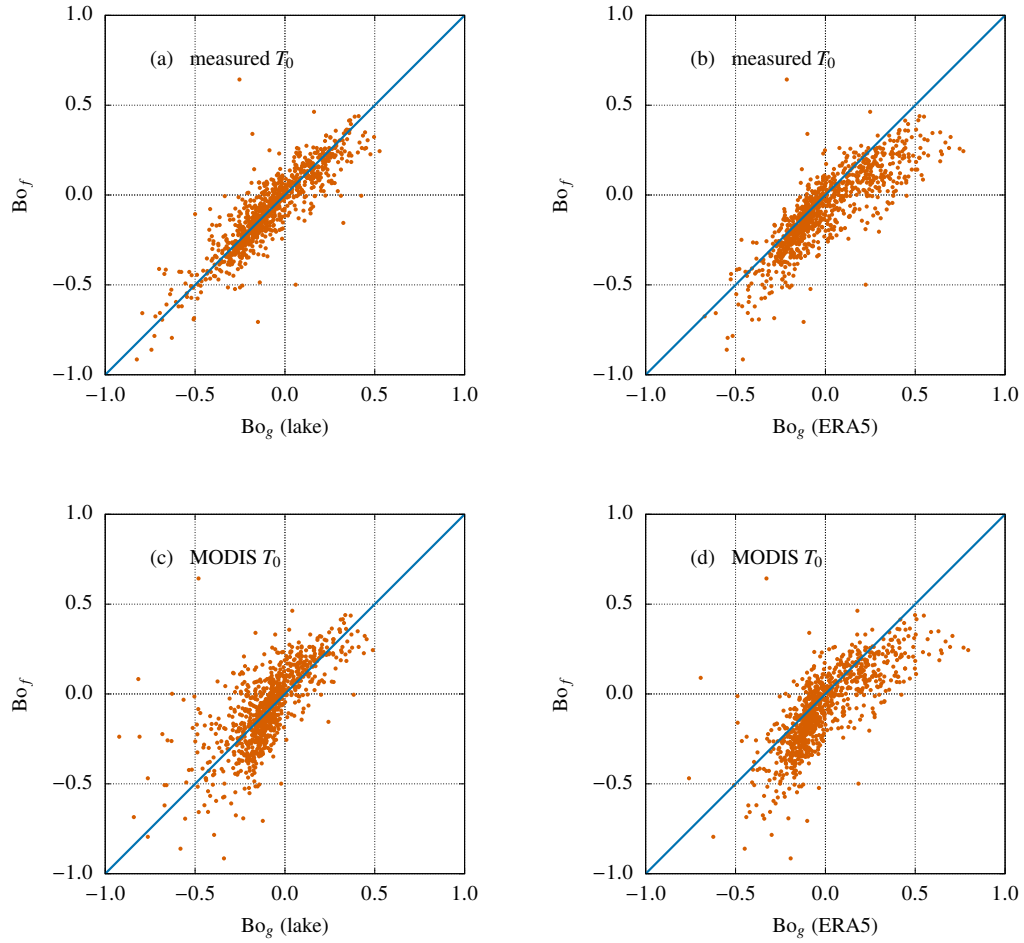


Figure 5. Comparison of $Bo_g \times Bo_f$. Upper row: Bo_g calculated from measured T_0 and over-water e_a and T_a (a) and Bo_g calculated from measured T_0 and land data e_a and T_a (b). Lower row: Bo_g calculated from MODIS T_0 and over-water e_a and T_a (c) and Bo_g calculated from MODIS T_0 and land data e_a and T_a (d).

370 of land-based air temperature and water vapor pressure may be generally acceptable in
 371 operational lake evaporation estimates.

Table 1. Values of a_B, b_B in Brutsaert (1975a)’s clear-sky atmospheric radiation equation available in the literated and tested in this study.

Source	a_B	b_B
(Brutsaert, 1975a)	0.643	0.1428
(Sugita & Brutsaert, 1993)	0.714	0.0687
(Duarte et al., 2006)	0.625	0.1310
(Choi et al., 2008)	0.626	0.1300

5 Model validation

5.1 Atmospheric radiation

The availability of remotely-sensed water surface temperatures and the advent of automated weather stations where R_s is routinely measured (or reanalysis datasets from which it can be retrieved), leaves R_a as the most uncertain term in net radiation estimates from (2). As we mentioned above, in this work we chose to estimate R_a instead of using reanalysis-derived values (which would further simplify the model), on the grounds that the use of data from a nearby meteorological station is likely to remain a common operational practice. The choice of models and parameters is still wide, however. Here, after deciding to use Brutsaert (1975a)’s equation (3) together with (4), one must consider which values of a_B, b_B and a_P, b_P to use. We tested 3 pairs of a_B, b_B reported in the literature and listed in Table 1: the original values proposed by Brutsaert (1975a); those found by Sugita and Brutsaert (1993) with FIFE data; and those obtained by Duarte et al. (2006), which are virtually identical to the values later found by Choi et al. (2008).

The values of a_P, b_P are used to obtain S , and then C , to estimate the increase in atmospheric radiation due to the presence of clouds in (4). This of course is not the original intended use of Prescott’s equation, but allows C to be obtained indirectly where manual observations are not available. Reported values of a_P, b_P are in the ranges $a_P \in [0.2, 0.3]$ and $b_P \in [0.475, 0.575]$ (Black et al., 1954; Glover & McCulloch, 1958), where we rounded the figures for simplicity. A brute-force search was made by testing, for each of the 3 pairs of a_B, b_B , 5 equally spaced values of a_P centered at 0.25, and 5 equally spaced values of b_P centered at 0.525, in a total of 75 possibilities, by calculating R_a in (2) and comparing the resulting estimated net radiation with the measured values. Performance

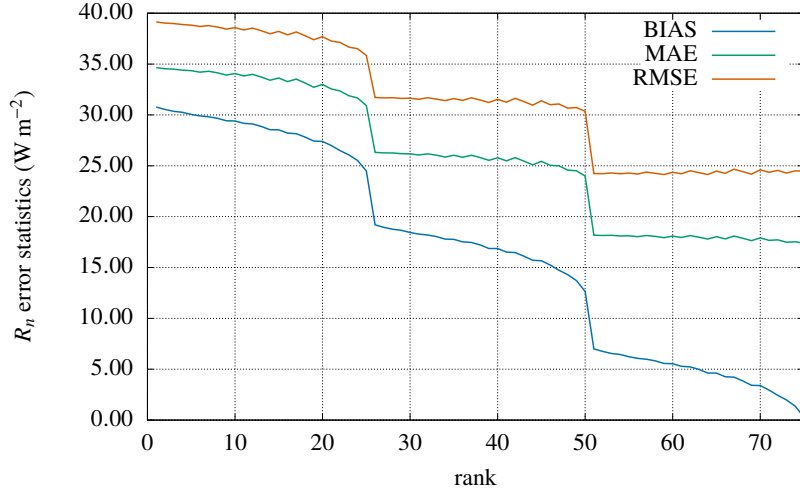


Figure 6. Error statistics of estimated net radiation as a function of model parameter choice: Bias (blue), Mean absolute error (green) and Root Mean Square Error (vermillion). The pronounced jumps indicate change in the clear-sky atmospheric radiation model parameters a_B , b_B .

395 statistics were calculated for each alternative: bias (BIAS), mean absolute error (MAE),
 396 root mean square error (RMSE), coefficient of correlation (r) and Willmott's refined in-
 397 dex of model performance (d_r), which can vary from -1 to $+1$, the latter figure mean-
 398 ing perfect prediction (Willmott et al., 2012). The 75 values were ranked by d_r . Inter-
 399 estingly, the ranking is organized by the clear-sky atmospheric radiation parameters. Thus,
 400 the best 25 alternatives use Sugita and Brutsaert (1993)'s values, followed by Brutsaert
 401 (1975a)'s values. The worst 25 alternatives use Duarte et al. (2006)'s values. Therefore,
 402 the sensitivity of the error to the particular pair of a_P , b_P is relatively small. This is sum-
 403 marized in Figure 6, where we plot BIAS, MAE and RMSE by rank, rank 1 being the
 404 worst value of d_r and rank 75 the best. The pronounced jumps in the figure represent
 405 changes of clear-sky model parameters from each of the aforementioned 3 choices of a_B , b_B .
 406 The best set of parameters is $a_P = 0.3000$, $b_P = 0.5750$, $a_B = 0.7140$, $b_B = 0.0687$,
 407 with $\text{BIAS} = -0.26 \text{ W m}^{-2}$, $\text{MAE} = 17.38 \text{ W m}^{-2}$, $\text{RMSE} = 24.49 \text{ W m}^{-2}$, $r = 0.9661$
 408 and $d_r = 0.8961$. Note that these values were found through, and therefore reflect, the
 409 use of daily instead of 30-minute or hourly data.

410 In some sense, net radiation estimates remain the Achilles's heel of evaporation mod-
 411 els based on available energy: most of these models rely on a net radiation parameter-

Table 2. The parameter θ in $f(u, \theta)$ found for each version of STAEBLE.

version	A	B	AB	C	CH
θ	A	B	$A/2, B/2$	z_0 (m)	a_C
	0.004210	0.001824	0.002105, 0.000912	0.008434	6.3246

412 ization with fixed values (*e.g.* Penman, 1948; Morton, 1983), and systematic errors in
413 net radiation estimates will be carried over to lake evaporation estimates. In all fairness,
414 the radiation parameterizations used in evaporation models should not be confused with
415 the models themselves. Figure 6 gives a realistic idea of the magnitude of the errors that
416 may be incurred if R_n estimates are not locally validated. In this work, we will adopt
417 the best set of radiation parameters found above in the STAEBLE model evaporation
418 estimates, thereby minimizing the errors induced by R_n estimates. It is important to note
419 that over-water measurements of R_n are not needed for this step: it is equally possible
420 to adjust the model with land-based measurements of R_a , as done by the aforementioned
421 studies by Sugita and Brutsaert (1993), Duarte et al. (2006) and Choi et al. (2008); our
422 use of R_n to obtain the best set of parameters was simply based on the fact that R_n data,
423 instead of R_a data, were readily available.

424 5.2 STAEBLE model performance

425 The 5 versions of STAEBLE described in section 2 were tested against the mea-
426 sured values of the latent heat flux. For completeness, the parameter θ found by solv-
427 ing (14) for each version of STAEBLE is listed in Table 2. Note that z_0 and a_C are *not*
428 representative of commonly reported over-water values, both because land-based T_a , e_a
429 and u are used and because they are daily averages. For a comparison, using an approx-
430 imate mean surface area of 370 km² for the first two years of study reported by M. T. Moreo
431 and Swancar (2013, Figure 8) in Harbeck (1962)’s equation gives a constant coefficient
432 of 0.001085 for the equivalent of B ; Brutsaert (1982, Chapter 5) gives a_C in the range
433 0.012–0.072 from various sources; Shabani et al. (2014) however found $a_C = 0.110$. For
434 the momentum roughness length, a typical value given by Brutsaert (1982, Chapter 5)
435 is $z_0 = 0.00023$ m, but a recent review of the drag coefficients for lakes (Guseva et al.,
436 2022) gives (for high wind speeds) $z_0 = 0.0013$ m.

Table 3. Error statistics for 5 versions of STAEBLE at the daily, 12-day and monthly time scales.

Time scale	Version	BIAS (W m^{-2})	MAE (W m^{-2})	RMSE (W m^{-2})	r	d_r
daily	STAEBLE-A	-2.63	54.43	73.64	0.4504	0.5363
	STAEBLE-B	+1.71	61.14	78.26	0.6628	0.4791
	STAEBLE-AB	-0.46	51.38	66.45	0.6253	0.5623
	STAEBLE-C	-4.80	46.53	62.61	0.7058	0.6035
	STAEBLE-CH	-3.00	50.50	67.86	0.7033	0.5698
12-day	STAEBLE-A	-2.64	33.44	41.34	0.7233	0.5820
	STAEBLE-B	+1.71	48.69	58.54	0.6912	0.3913
	STAEBLE-AB	-0.47	38.70	47.11	0.7222	0.5163
	STAEBLE-C	-4.81	24.41	31.47	0.8568	0.6948
	STAEBLE-CH	-3.00	26.33	34.36	0.8450	0.6708
monthly	STAEBLE-A	-2.69	29.02	35.79	0.7832	0.6063
	STAEBLE-B	+1.60	47.49	55.02	0.7036	0.3559
	STAEBLE-AB	-0.55	36.63	43.49	0.7524	0.5032
	STAEBLE-C	-4.83	20.15	25.75	0.8855	0.7267
	STAEBLE-CH	-3.03	22.44	28.24	0.8732	0.6957

437 The model runs at the daily time scale, after which error statistics are calculated
438 for 3 time scales: daily, 12 days, and monthly. A LOWESS (locally weighted scatterplot
439 smoothing) low-pass filter (Cleveland, 1979, 1981; Cleveland & Devlin, 1988) with a tri-
440 cubic weighting function $w(x) = (1 - |x|^3)^3$ (Figueira, 2019) was applied to the daily
441 *LE* data, using a window size of 21 days. Because LOWESS employs weighted linear re-
442 gression, weighing more heavily the data points closest to the time at which the filtered
443 data are calculated, this actually corresponds to a somewhat smaller *actual* time scale.
444 Putting $\int_{-1}^{+1} w(x) dx = 1 \times \Delta x$, where Δx is the effective scale of the independent vari-
445 able, gives $\Delta x = 81/140$, which translates to a time scale of $11.57 \approx 12$ days.

446 The error statistics are shown in Table 3, and highlight the second main result of
447 this work, which is the critical importance of atmospheric stability in mass transfer lake
448 evaporation modeling. Thus, STABLE-B, which has the same analytical form of Harbeck

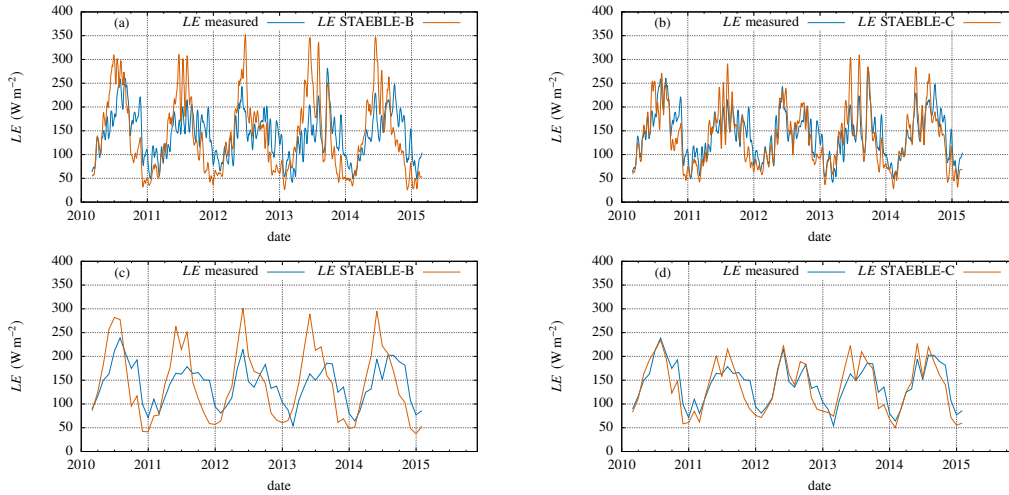


Figure 7. Comparison of the worst (STAEBLE-B) and best (STAEBLE-C) versions of the STAEBLE framework. (a) STAEBLE-B, 12-day timescale; (b) STAEBLE-C, 12-day timescale; (c) STAEBLE-B, monthly time scale and (d) STAEBLE-C, monthly time scale.

449 (1962)'s equation, has the largest MAE and RMSE of the 5. Moreover, its performance
 450 index d_r decreases with increasing timescale, the same happening, unsurprisingly, to STAEBLE-
 451 AB. Note that the important role of stability had already been verified with over-lake
 452 data at the 30 min – 1 h time scale by Verburg and Antenucci (2010), but now is extended
 453 to the daily time scale and over-land meteorological data. While all existing lake evap-
 454 oration models for hydrological purposes (to the best of our knowledge) use a mass trans-
 455 fer function of the type (15), (17) or (19), with constant A and/or B , the incorporation
 456 of standard atmospheric stability effects produces a pronounced increase in overall model
 457 performance. Except for BIAS, STAEBLE-C shows the best set of performance statis-
 458 tics for all three time scales.

459 We show the worst and best versions for the 12-day and monthly time scales in Fig-
 460 ure 7. Note that (17) and (28) share the same form (a coefficient multiplying the daily
 461 wind speed u), with the coefficient being constant in STAEBLE-B, and varying daily with
 462 atmospheric stability in STAEBLE-C: the improvement obtained by incorporating at-
 463 mospheric stability into the model is again evident. Therefore, it is recommended that
 464 STAEBLE-C, which is slightly simpler than STAEBLE-CH, be adopted for operational
 465 purposes.

6 Discussion and conclusions

Perhaps the three main issues regarding lake evaporation models have been: (i) the degree of error introduced by using over-land data; (ii) the need to apply a transfer coefficient calibrated elsewhere; and (iii) the need to estimate the rate-of-change of enthalpy D . In this work, using data from Lake Mead, we have shown that (i) is not critical, and that good estimates can be obtained with land-based data. Moreover, we have introduced a new (but very simple) way to calibrate the transfer coefficient $f(u, \theta)$ by enforcing the closure of the long-run energy budget, when the cumulative value of D becomes negligible in comparison to the other terms. We emphasize that the calibration procedure does not require *in-situ* measurements of lake evaporation. We have also shown that a constant-value transfer coefficient, even if calibrated locally, although able to reproduce the average annual evaporation, performs relatively poorly at the monthly and smaller time scales. Our results show that this is caused by changes in atmospheric stability over the year. We have shown that adjusting for atmospheric stability using standard and widely accepted MOST stability functions (which do not need to be locally calibrated) solves this issue. Overall, then, (ii) is solved. The result is a model that uses a small set of data, is able to calculate H and LE with the heat and mass transfer approach (therefore dispensing with estimates of D , which solves (iii)), and is locally calibrated, which means that local effects including lake size are automatically incorporated. The model can be applied at any location where the required input data are available.

As it happens with all lake evaporation models based on available energy, good estimates of R_n impact directly on the long-term LE estimates produced by the model. It is possible to verify the quality of the R_s data and R_a estimates with simultaneous over-land measurements (or use measured data directly in the model), and this should be considered, whenever possible, for best results.

The importance of using MODIS water surface temperature data cannot be overemphasized, since STAEBLE hinges critically on them to derive its lake evaporation estimates. The small underestimation of T_0 at Lake Mead by MODIS during winter should be more closely investigated in the future.

495 **Appendix A Adopted Businger-Dyer integral MOST functions**

496 For stable conditions ($\zeta > 0$),

$$497 \Psi_s(\zeta) = \Psi_u(\zeta) = \begin{cases} -5\zeta & \zeta \leq 1, \\ -5 & \zeta > 1. \end{cases} \quad (\text{A1})$$

498 For unstable conditions ($\zeta \leq 0$),

$$499 x = (1 - 16\zeta)^{1/4}, \quad (\text{A2})$$

$$500 \Psi_u(\zeta) = 2 \ln \left[\frac{(1+x)}{2} \right] + \ln \left[\frac{(1+x^2)}{2} \right] - 2 \arctan(x) + \frac{\pi}{2}, \quad (\text{A3})$$

$$501 \Psi_s(\zeta) = 2 \ln \left[\frac{(1+x^2)}{2} \right]. \quad (\text{A4})$$

502

503 **Open Research**

504 All input data used in this research are publicly available at the ERA5 repository
 505 according to the licence to use Copernicus Products (Hersbach et al., 2018), the AQUA
 506 and TERRA MODIS repositories (Wan et al., 2021a, 2021b) and the USGS Lake Mead
 507 Study data repository (M. Moreo, 2015). The processed data are available at Dias et al.
 508 (2022).

509 **Acknowledgments**

510 We are deeply grateful to the USGS and all USGS personnel involved in the Lake
 511 Mead 2010–2015 study whose data are used herein, without which this research would
 512 not have been possible.

513 This study was funded by FUNPAR research grants, 03638 e 03955, both funded
 514 by the Brazilian Agência Nacional de Águas (National Water Agency), ANA.

515 We thank Henrique F. Duarte for his careful reading of the manuscript and many
 516 suggestions that helped to improve it.

517 **References**

- 518 Armani, F. A. S., Dias, N. L., & Damázio, J. M. (2020). Eddy-covariance CO₂ fluxes
 519 over Itaipu Lake, southern brazil. *Rev Bras Rec Hídr*, 25, 1–14.
- 520 Assouline, S., & Mahrer, Y. (1993). Evaporation from lake Kinneret 1. Eddy corre-
 521 lation system measurements and energy budget estimates. *Water Resour Res*,

- 522 29(4), 901–910.
- 523 Black, J., Bonython, C., & Prescott, J. (1954). Solar radiation and the duration of
524 sunshine. *Q J R Meteorol Soc*, 80(344), 231–235.
- 525 Blanken, P. D., Rouse, W. R., Culf, A. D., Spence, C., Boudreau, L. D., Jasper,
526 J. N., . . . Verseghy, D. (2000). Eddy covariance measurements of evaporation
527 from Great Slave Lake, Northwest Territories, Canada. *Water Resour Res*,
528 36(4), 1069–1077.
- 529 Bowen, I. S. (1926). The ratio of heat losses by conduction and by evaporation from
530 any water surface. *Phys Rev*, 27, 779–787.
- 531 Brutsaert, W. (1975a). On a derivable formula for long-wave radiation from clear
532 skies. *Water Resour Res*, 11, 742–744.
- 533 Brutsaert, W. (1975b). The roughness length for water vapor, sensible heat and
534 other scalars. *J Atmos Sci*, 32, 2028–2031.
- 535 Brutsaert, W. (1982). *Evaporation into the atmosphere*. Dordrecht: D. Reidel. (309
536 pp.)
- 537 Brutsaert, W., & Yeh, G.-T. (1970). Implications of a type of empirical evaporation
538 formula for lakes and pans. *Water Resour Res*, 6, 1202–1209.
- 539 Cancelli, D. M., Dias, N. L., & Chamecki, M. (2012). Dimensionless criteria
540 for the production-dissipation equilibrium of scalar fluctuations and their
541 implications for scalar similarity. *Water Resour Res*, 48, W10522. doi:
542 10.1029/2012WR012127
- 543 Choi, M., Jacobs, J. M., & Kustas, W. P. (2008). Assessment of clear and cloudy
544 sky parameterizations for daily downwelling longwave radiation over different
545 land surfaces in florida, usa. *Geophys Res Lett*, 35(20).
- 546 Cleveland, W. S. (1979). Robust locally weighted regression and smoothing scatter-
547 plots. *J Am Stat Assoc*, 74(368), 829–836.
- 548 Cleveland, W. S. (1981). Lowess: A program for smoothing scatterplots by robust
549 locally weighted regression. *Am Stat*, 35(1), 54.
- 550 Cleveland, W. S., & Devlin, S. J. (1988). Locally weighted regression: an approach
551 to regression analysis by local fitting. *J Am Stat Assoc*, 83(403), 596–610.
- 552 COESA. (1976). *U.S. Standard Atmosphere, 1976*. (Tech. Rep.). U.S. Government
553 Printing Office.
- 554 Cogley, J. G. (1979). The albedo of water as a function of latitude. *Mon Wea Rev*,

555 107(6), 775–781.

556 DelSontro, T., Beaulieu, J. J., & Downing, J. A. (2018). Greenhouse gas emissions
557 from lakes and impoundments: Upscaling in the face of global change. *Limnol*
558 *Oceanogr Lett*, 3(3), 64–75.

559 Dias, N. L., Hoeltgebaum, L. E. B., & Santos, I. (2022). *Dataset for ‘STAE-*
560 *BLE: A surface-temperature- and available-energy-based lake evapora-*
561 *tion model’ article, HydroShare*. Retrieved from [https://doi.org/](https://doi.org/10.4211/hs.fa49d7f16703447b9e04552cc532936d)
562 [10.4211/hs.fa49d7f16703447b9e04552cc532936d](https://doi.org/10.4211/hs.fa49d7f16703447b9e04552cc532936d) doi: 10.4211/
563 [hs.fa49d7f16703447b9e04552cc532936d](https://doi.org/10.4211/hs.fa49d7f16703447b9e04552cc532936d)

564 Dias, N. L., & Reis, R. J. (1998). Métodos de cálculo do balanço de entalpia em la-
565 gos e erros associados (in Portuguese). *Rev Bras Rec Hídr*, 3(3), 45–56.

566 Dias, N. L., & Vissotto, D. (2017). The effect of temperature-humidity similar-
567 ity on bowen ratios, dimensionless standard deviations, and mass transfer
568 coefficients over a lake. *Hydrol Process*, 31(2), 256–269. Retrieved from
569 <http://dx.doi.org/10.1002/hyp.10925> doi: 10.1002/hyp.10925

570 Duarte, H. F., Dias, N. L., & Maggiotto, S. R. (2006). Assessing daytime downward
571 longwave radiation estimates for clear and cloudy skies in Southern Brazil.
572 *Agric For Meteorol*, 139, 171–181. doi: 10.1016/j.agrformet.2006.06.008

573 Figueira, J. P. (2019). *LOESS smoothing data using local regression*. Retrieved from
574 <https://towardsdatascience.com/loess-373d43b03564>

575 Glover, J., & McCulloch, J. (1958). The empirical relation between solar radiation
576 and hours of sunshine. *Q J R Meteorol Soc*, 84(360), 172–175.

577 Guseva, S., Armani, F., Desai, A., Dias, N. L., Eugster, W., Iwata, H., ... Lorke,
578 A. (2022). Bulk transfer coefficients estimated from eddy-covariance measure-
579 ments over lakes and reservoirs. *Submitted to J Geophys Res*.

580 Harbeck, G. E., Jr. (1962). *A practical field technique for measuring reservoir evap-*
581 *oration utilizing mass-transfer theory* (Professional Paper Nos. 272-E). U. S.
582 Geological Survey. Available at [https://pubs.usgs.gov/pp/0272e/report](https://pubs.usgs.gov/pp/0272e/report.pdf)
583 [.pdf](https://pubs.usgs.gov/pp/0272e/report.pdf).

584 Hersbach, H., Bell, B., Berrisford, P., Biavati, G., Horányi, A., Muñoz Sabater, J.,
585 ... Thépaut, J.-N. (2018). *ERA5 hourly data on single levels from 1979*
586 *to present. Copernicus Climate Change Service (C3S) Climate Data Store*
587 *(CDS)*. [dataset]. Retrieved from <https://cds.climate.copernicus.eu/>

- 588 cdsapp#!/dataset/reanalysis-era5-single-levels?tab=form doi:
589 10.24381/cds.adbb2d47
- 590 Hostetler, S. W., & Bartlein, P. J. (1990, October). Simulation of lake evaporation
591 with application to modeling lake level variations of Harney-Malheur Lake,
592 Oregon. *Water Resour Res*, *26*(10), 2603-2612.
- 593 Kohler, M., & Parmele, L. (1967). Generalized estimates of free-water evaporation.
594 *Water Resour Res*, *3*, 997-1005.
- 595 Lang, A., Mcnaughton, K., Fazu, C., Bradley, E., & Ohtaki, E. (1983). Inequality
596 of eddy transfer coefficients for vertical transport of sensible and latent heats
597 during advective inversions. *Boundary-Layer Meteorol*, *25*, 25-41.
- 598 McJannet, D. L., Webster, I. T., & Cook, F. J. (2012). An area-dependent wind
599 function for estimating open water evaporation using land-based meteorologi-
600 cal data. *Environ Modell Softw*, *31*, 76-83.
- 601 Montgomery, R. B. (1947). Viscosity and thermal conductivity of air and diffusivity
602 of water vapor in air. *J of Meteorology*, *4*, 193-196.
- 603 Moreo, M. (2015). *Evaporation data from Lake Mead and Lake Mohave, Nevada*
604 *and Arizona, March 2010 through April 2015* [U.S. Geological Survey Data
605 Release]. Retrieved from <http://dx.doi.org/10.5066/F79C6VG3>
- 606 Moreo, M. T., & Swancar, A. (2013). *Evaporation from Lake Mead, Nevada and*
607 *Arizona, March 2010 through February 2012* (Scientific Investigations Report
608 No. 2013-5229). Reston, Virginia: U.S. Geological Survey.
- 609 Morton, F. I. (1983). Operational estimates of lake evaporation. *J Hydrol*, *66*, 77-
610 100.
- 611 Morton, F. I. (1986). Practical estimates of lake evaporation. *J Appl Meteorol*, *25*,
612 371-387.
- 613 Obukhov, A. M. (1946 1971). Turbulence in an atmosphere with non-uniform tem-
614 perature. *Boundary-Layer Meteorol*, *2*, 7-29.
- 615 Omar, M., & El-Bakry, M. (1981). Estimation of evaporation from the lake of the
616 aswan high dam (lake nasser) based on measurements over the lake. *Agr Forest*
617 *Meteorol*, *23*, 293-308.
- 618 Penman, H. (1948). Natural evaporation from open water, bare soil and grass. *P*
619 *Roy Soc London*, *A*(193), 120-146.
- 620 Prata, A. J. (1996). A new long-wave formula for estimating downward clear-sky ra-

- 621 diation at the surface. *Q J Roy Meteorol Soc*, *122*, 1127–1151.
- 622 Priestley, C. H. B., & Taylor, R. J. (1972). On the assessment of surface heat
623 flux and evaporation using large scale parameters. *Monthly Weather Review*,
624 *100*(2), 80–92.
- 625 Reis, R. J., & Dias, N. L. (1998). Multi-season lake evaporation: energy-budget
626 estimates and CRLE model assessment. *J Hydrol*, *208*, 135–147. Re-
627 trieved from [https://doi.org/10.1016/S0022-1694\(98\)00160-7](https://doi.org/10.1016/S0022-1694(98)00160-7) doi:
628 10.1016/S0022-1694(98)00160-7
- 629 Sellers, W. D. (1965). *Physical climatology*. Chicago: The University of Chicago
630 Press.
- 631 Shabani, B., Nielsen, P., & Baldock, T. (2014). Direct measurements of wind stress
632 over the surf zone. *J Geophys Res-Oceans*, *119*, 2949–2973.
- 633 Sugita, M., & Brutsaert, W. (1993). Cloud effect in the estimation of instantaneous
634 downward longwave radiation. *Water Resour Res*, *29*(3), 599–605.
- 635 Swinbank, W. C. (1951). Measurement of vertical transfer of heat and water vapor
636 by eddies in the lower atmosphere. *J Meteorol*, *8*, 135–145.
- 637 USGS. (1954). *Water-loss investigations: Lake hefner studies* (Geol. Surv. Prof. Pa-
638 per No. 269). U. S. Geological Survey.
- 639 USGS. (1958). *Water-loss investigations: Lake mead studies* (Geol. Surv. Prof. Pa-
640 per No. 298). U. S. Geological Survey.
- 641 van Flandern, T. C., & Pulkkinen, K. F. (1979, November). Low-precision formu-
642 lae for planetary positions. *Astrophys J SupplS*, *41*, 391–411. doi: 10.1086/
643 190623
- 644 Veldkamp, T., Wada, Y., Aerts, J., Döll, P., Gosling, S. N., Liu, J., . . . others
645 (2017). Water scarcity hotspots travel downstream due to human interven-
646 tions in the 20th and 21st century. *Nat Commun*, *8*(1), 1–12.
- 647 Verburg, P., & Antenucci, J. P. (2010). Persistent unstable atmospheric bound-
648 ary layer enhances sensible and latent heat loss in a tropical great lake: Lake
649 Tanganyika. *J Geophys Res-Atmos*, *115*(D11), D11109. Retrieved from
650 <http://dx.doi.org/10.1029/2009JD012839> doi: 10.1029/2009jd012839
- 651 Wan, Z., Hook, S., & Hulley, G. (2021a). *MODIS/Aqua Land Surface Tempera-*
652 *ture/Emissivity Daily L3 Global 1km SIN Grid V061* [dataset]. Retrieved from
653 <https://doi.org/10.5067/MODIS/MYD11A1.061> (NASA EOSDIS Land Pro-

- 654 cesses DAAC) doi: 10.5067/MODIS/MYD11A1.061
- 655 Wan, Z., Hook, S., & Hulley, G. (2021b). *MODIS/Terra Land Surface Tempera-*
656 *ture/Emissivity Daily L3 Global 1km SIN Grid V061* [dataset]. Retrieved from
657 <https://doi.org/10.5067/MODIS/MOD11A1.061> (NASA EOSDIS Land Pro-
658 cesses DAAC) doi: 10.5067/MODIS/MOD11A1.061
- 659 Wang, W., Lee, X., Xiao, W., Liu, S., Schultz, N., Wang, Y., ... Zhao, L. (2018).
660 Global lake evaporation accelerated by changes in surface energy allocation in
661 a warmer climate. *Nat Geosci*, *11*(6), 410–414.
- 662 Williamson, C. E., Dodds, W., Kratz, T. K., & Palmer, M. A. (2008). Lakes and
663 streams as sentinels of environmental change in terrestrial and atmospheric
664 processes. *Front Ecol Environ*, *6*(5), 247–254.
- 665 Willmott, C. J., Robeson, S. M., & Matsuura, K. (2012). A refined index of model
666 performance. *International Journal of Climatology*, *32*(13), 2088–2094.
- 667 Yang, D., & Bright, J. M. (2020). Worldwide validation of 8 satellite-derived and re-
668 analysis solar radiation products: A preliminary evaluation and overall metrics
669 for hourly data over 27 years. *Sol Energy*, *210*, 3–19.
- 670 Zhao, G., Gao, H., & Cai, X. (2020). Estimating lake temperature profile and evap-
671 oration losses by leveraging MODIS LST data. *Remote Sen Environ*, *251*,
672 112104.